YbPd$_2$In: A promising candidate for strong entropy accumulation at very low temperature

F. Gastaldo,[1] S. Gabáni,[2] A. Džubinská,[3] M. Reiffers,[4] G. Pristáš ,[2] I. Čurlík,[4] P. Skyba,[2] M. Clovecko,[2] F. Vavrek,[2]
J. G. Sereni,[5,*] and M. Giovannini[1]

[1]*Department of Chemistry, University of Genova, Via Dodecaneso 31, Genova, Italy*
[2]*Institute of Experimental Physics, SAS, Watsonova 47 Košice, Slovakia*
[3]*Faculty of Science, P.J. Šafárik University, Košice, Slovakia*
[4]*Faculty of Humanities and Natural Sciences, University of Prešov, 17. novembra 1, Prešov, Slovakia*
[5]*Low Temperature Division, CAB-CNEA, 8400 San Carlos de Bariloche, Argentina*

We report on synthesis, crystal structure, magnetic, thermodynamic, and transport properties of the compound YbPd$_2$In, crystallizing as a Heusler structure type. A trivalent state of the rare earth was determined by fitting the magnetic susceptibility with a Curie-Weiss law. This compound is characterized by showing very weak magnetic interactions and a negligible Kondo effect. A specific-heat jump was observed at $T \approx 250$ mK, followed at higher temperature by a power-law decrease of $C_P(T)/T$. The resulting large electronic entropy increase at very low temperature is rapidly shifted to higher temperature by the application of magnetic field. This magnetocaloric effect places YbPd$_2$In as a very good candidate for adiabatic demagnetization cooling processes.

I. INTRODUCTION

For decades, cerium and ytterbium intermetallics have attracted continuous attention owing to the variety of anomalous physical phenomena discovered on their compounds [1–4]. Recently notable examples of unique properties have been found in the Yb-T-X systems (T = transition metals, X = p-type elements). For instance, in a systematic search for new ytterbium-palladium indides and stannides [5,6], Yb$_2$Pd$_2$Sn has been synthesized, where two quantum critical points (QCPs) occur under pressure [7,8] and at Sn/In doping [9].

Prominent examples with platinum are given by the hexagonal YbPt$_2$Sn and the cubic Heusler YbPt$_2$In [10]. Although crystal structures are different, these two compounds exhibit many common features, like stable trivalent Yb^{3+} magnetic moments in a framework of negligible Kondo effect and very weak exchange interactions. Moreover, both compounds are characterized by similar trends of C_m/T by temperature decreasing: an increase of $C_m(T)/T$ according to a power-law dependence below 2 K followed by broad anomalies at around 200 mK. It is worth noting that in these compounds C_m/T reaches record values up to 14 J/mol K^2. Similar features were found in YbCu$_{5-x}$Au$_x$ ($0.4 < x < 0.7$), YbCo$_2$Zn$_{20}$, and YbBiPt, but showing a plateau in C_m/T ($T \to 0$) at ≈ 7 J/mol K^2 [11–13], all implying high values of entropy increase at very low temperature.

The current interpretation for these unusual behaviors is that long-range magnetic order is inhibited by very weak magnetic exchange or by magnetic frustration of Yb atoms placed in two-dimensional (2D) (triangular) or 3D (tetrahedra)

networks. Coincidentally, only very low Kondo effect affects their robust magnetic moments.

In some of these compounds, e.g., YbPt$_2$Sn and YbPt$_2$In [10], it was shown that the low-temperature magnetic entropy is strongly shifted to higher temperature by applying magnetic fields, offering the interesting perspective to use these materials as efficient metallic refrigerant for adiabatic magnetization cooling [8,14].

In this work we report experimental results on crystal structure and physical properties of the cubic Heusler indide YbPd$_2$In which, based on the present results of this paper, behaves similarly to the other members of the (T = Pt or Pd and X = Sn or In) family of compounds. Previous study, restricted to magnetization and inelastic neutron studies [15], only provides the crystal electric-field parameters in cubic symmetry.

II. EXPERIMENTAL DETAILS

YbPd$_2$In polycrystalline samples, each with a total weight of 1.2 g, have been prepared by weighting the stoichiometric amount of elements with the following nominal purity: Yb-99.993 mass % (pieces, Yb/TREM purity, Smart Elements GmbH, Vienna, Austria), Pd-99.5 mass % (foil, Chimet, Arezzo, Italy), In-99.999 mass % (bar, Smart Elements GmbH, Vienna, Austria). In order to avoid the loss of ytterbium during the melting because of their high vapor pressure, the proper amounts of pure elements were enclosed in small tantalum crucibles sealed by arc welding under pure argon atmosphere. The samples were synthesized in an induction furnace under a stream of pure argon and annealed in a resistance furnace at 750 °C for two weeks. Finally the samples were quenched in cold water and characterized by optical and scanning electron microscopy (SEM) (EVO 40,
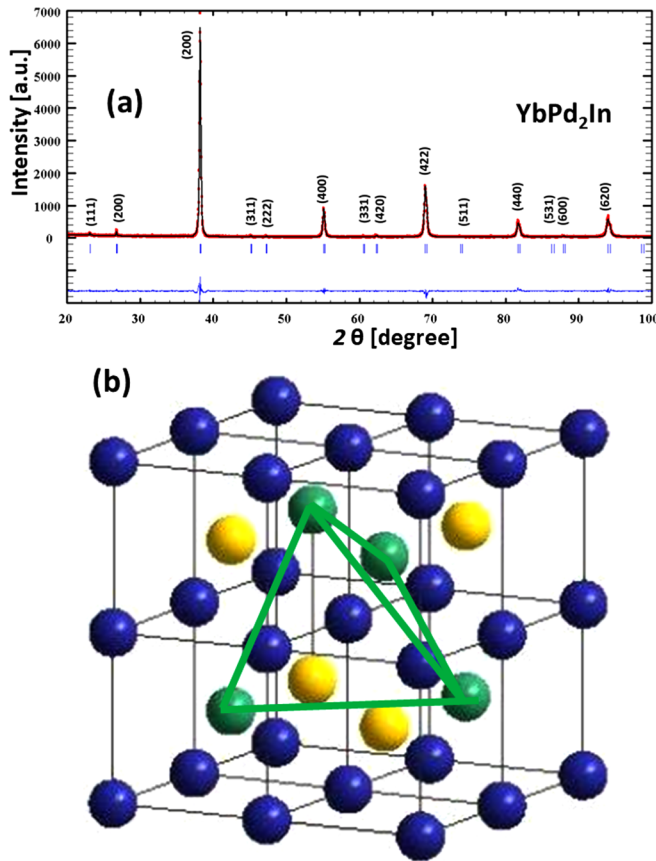
———————
*jsereni@yahoo.com

FIG. 1. (a) The experimental powder x-ray-diffraction pattern for YbPd$_2$In at room temperature compared with the calculated diffraction diagram. Experimental data are shown by symbols, whereas the line through the data represents the results of the Rietveld refinement. The lower curve is the difference among them. The ticks indicate respective Bragg peak positions, indicated by Miller indices. All reflexes were indexed according to the cubic Heusler phase structure type. (b) In YbPd$_2$In, of Cu$_2$MnAl-type structure, Yb atoms (green in the figure) form a network of edge-sharing tetrahedra like a 3D analog of a triangular lattice. In (yellow) and Pd (blue) are also depicted.

Carl Zeiss, Cambridge, England), equipped with an electron probe microanalysis system based on energy dispersive x-ray spectroscopy (EPMA EDXS). For the quantitative and qualitative analysis an acceleration voltage of 20 keV for 100 s was applied, and a cobalt standard was used for calibration. The x-ray intensities were corrected for atomic number, absorption, and fluorescence effects. The annealed samples were crushed, powdered under pure acetone inside an agate mortar and studied by powder x-ray diffraction (XRD). The XRD data were collected at room temperature using the X-Pert MPD diffractometer (Philips, Almelo, The Netherlands) equipped with a graphite monochromator installed in the diffracted beam (Bragg Brentano, CuKα radiation). Rietveld matrix full-profile refinements were performed using the program FULLPROF [16].

In the 2-300-K temperature range, thermodynamic, transport, and magnetic properties were performed by physical property measurement system (PPMS) Dynacool (Quantum Design) with applied magnetic field up to 9 T. Electrical resistivity and magnetoresistance were measured using the four-wire AC technique. For magnetic measurements the vibrating magnetometer technique VSM was used, whereas AC susceptibility was measured in MPMS (Quantum Design). Specific heat was determined by means of the 2-τ relaxation method. Under applied magnetic fields, in the temperature range 0.4–8 K and up to 9 T, they were carried out using a PPMS (Quantum Design). In the temperature range below 1 K down to 80 mK a ^{3}He-^{4}He dilution cryogen-free refrigerator (TRITON 200, Oxford Instruments, UK) was used under fields up to 1.2 T.

III. EXPERIMENTAL RESULTS

A. Crystal structure

In the course of a systematic investigation of the ternary Yb-Pd-In system a different ternary phase was found. A sample prepared on the stoichiometry 1:2:1 from SEM/EPMA revealed to be a practically single phase. In fact, the XRD pattern of the compound was successfully indexed by analogy with the corresponding known cubic phase YbPd$_2$Sn, which crystallizes with $cF16$ structure Cu$_2$MnAl-type (space group $Fm\bar{3}m$). The structural Rietveld profile fitting is shown in Fig. 1(a). A lattice parameter $a = 6.6605(1)$ Å was obtained. Reasonable reliability factors were obtained for the fully ordered structure ($R_B = 3.07\%$, $R_F = 2.62\%$, $R_P = 9.07\%$), excluding the presence of strong disorder. Moreover, in agreement to SEM results, in the XRD pattern no peaks belonging to spurious phases were found.

Analyzing the spatial coordination of Yb magnetic atoms in the Cu$_2$MnAl-type structure, one sees in Fig. 1(b) that Yb nearest neighbors are located in tetrahedral coordination (indicated with green lines) with the proper geometrical conditions for a 3D magnetic frustration scenario, provided an antiferromagnetic Yb-Yb magnetic exchange.

B. Magnetic properties

The temperature dependence of $1/\chi(T)$ inverse magnetic susceptibility for YbPd$_2$In is shown in Fig. 2. The measurements were done in a magnetic field of 1 T in the temperature range between 2 and 300 K. The susceptibility data can be accounted for with a modified Curie-Weiss (CW) law given by the equation

$$\chi(T) = \chi_0 + \frac{c}{T - \Theta_P}. \tag{1}$$

From the high-temperature fitting of the dependence $1/\chi(T)$ the value of the effective moment for YbPd$_2$In is $\mu_{\text{eff}} = 4.49\mu_B$, which is close to the free Yb^{3+} value $\mu_{\text{eff}} = 4.54\mu_B$. The paramagnetic Curie temperature obtained from the fit is $\Theta_p = -9$ K which is an indication of antiferromagnetic exchange interactions. Notably, no Pauli-like contribution χ_0 is detected from this $1/\chi(T)$ dependence. Magnetization measurements up to 5 T performed between 2 K and room temperature [15] are in agreement with the susceptibility results.
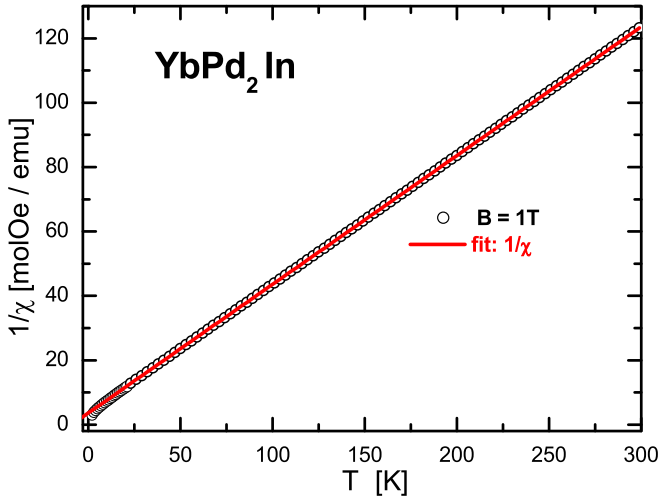
FIG. 2. Temperature dependence of inverse susceptibility of YbPd$_2$In.

C. Electrical resistivity

The normalized temperature dependence of electrical resistivity ($\rho(T)/\rho_{300\,K}$) of YbPd$_2$In, measured at magnetic fields of 0 and 6 T, is shown in Fig. 3. The residual resistivity ratio RRR ~ 5.5 indicates a good quality of the polycrystalline sample, improving the RRR ~ 2.2 value of the YbPt$_2$Sn compound [10] (the comparison with YbPt$_2$In is meaningless because this compound undergoes a CDW transition).

Focusing on the positive curvature of $\rho(T)$ at low temperatures, the question arises about a coherent regime below 25 K. This feature is confirmed by the linear thermal variation of the $\delta\rho/\delta T$ derivative, which corresponds to the $\rho(T) = \rho_0 + AT^2$ dependence of a Fermi liquid (see the straight line in Fig. 3). On the other hand, the broad negative curvature centered around 70 K can be attributed to strongly hybridized crystal electric-field excited levels [15]. The linear T dependence of
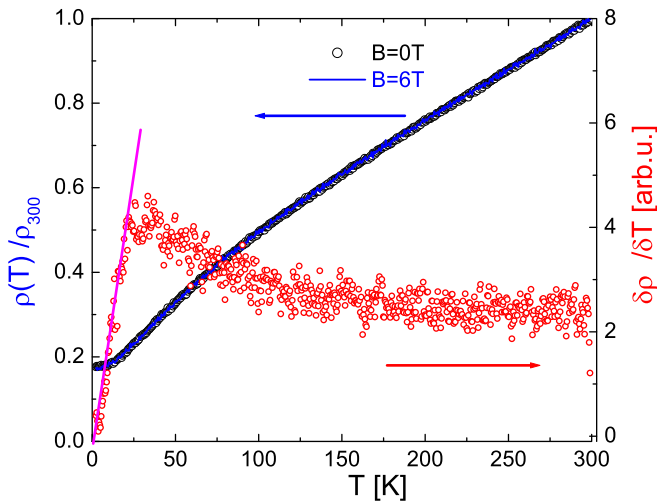

FIG. 3. Left axis: temperature dependence of electrical resistivity of YbPd$_2$In normalized to room (300 K) temperature. Right axis: electrical resistivity derivative showing a nearly linear increase between zero and about 25 K.
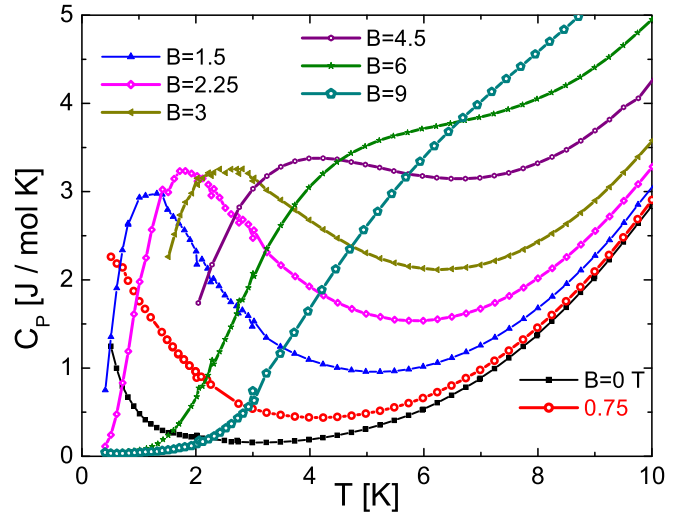

FIG. 4. Temperature dependence of the specific heat of YbPd$_2$In at zero and applied field up to $B = 9$ T.

$1/\chi(T)$ shown in Fig. 2 agrees with that scenario. Moreover, practically no magnetoresistance effect was detected. In fact, applied fields of $B = 3$ T (not shown) and 6 T produce no detectable effect on the $\rho(T)$ dependence.

D. Specific heat

In Fig. 4 the specific-heat $C_P(T, B)$ measurements performed at $0.5 < T < 10$ K at different magnetic fields up to $B = 9$ T are presented. The specific-heat upturns for $B \leqslant 0.75$ T reveal an arising anomaly which reaches its maximum at $T_{\max} = 1.2$ K for $B = 1.5$ T and continues to increase proportionally to the field intensity: $T_{\max}(B)$ K $\propto B$. On the other hand, the height of the maximum barely increases. These anomalies can be properly described as Schottky-type anomalies only above $B = 4$ T once the specific heat reaches the expected value of 3.6 J/mol K corresponding to a two-level system split by applied field behavior. Although $T_{\max}(B > 4$ T) extrapolates to zero for $B \to 0$, in the magnetic phase diagram shown in Fig. 9 one sees the $T_{\max}(B)$ dependence turns down at low fields indicating the rising of low-energy magnetic correlations which will be analyzed in the following section. Above the anomaly $C_P(T > 6$ K, $B)$ grows significantly with increasing field, suggesting an incipient contribution of the excited crystal electric-field levels.

The specific-heat measurement at very low temperature in zero field is depicted in Fig. 5 in a double logarithmic representation. Since at $T < 3$ K the phonon contribution is negligible, in the text we will refer to the magnetic contribution as C_P/T or C_m/T indistinctly. On the other side, the nuclear contribution C_n is can be considered irrelevant at $T \approx 0.1$ in zero field. The trend of the curve is characterized by three features: a C_m/T jump picking at $T \approx 210$ mK, a power-law dependence that properly describes the thermal decrease between 260 mK and 3 K, and a small jump at $T = 2.2$ K. The C_m/T jump observed at $210 < T < 260$ mK indicates a magnetic transition that involves the Yb-$4f$ electrons, whose nature will be analyzed tracing its phase boundary dependence under applied magnetic field. At 0.3 K $\leqslant T \leqslant 3$ K, C_m/T can
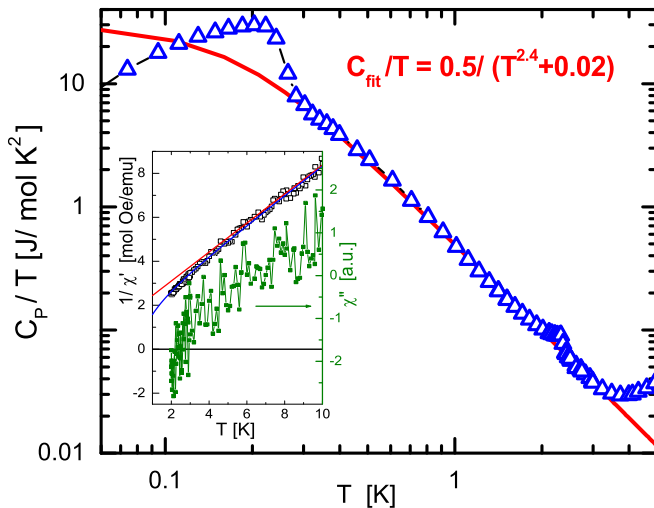
FIG. 5. Very low-temperature $C_P(T)/T$ variation at zero field for YbPd$_2$In in a double logarithmic representation. The continuous curve C_{fit}/T represents a modified power-law thermal dependence obtained within the 0.28 K $< T <$ 3 K range. Inset: Detail of the low-temperature AC susceptibillity: inverse of the inductive component (left axis) and the dissipative one (right axis).
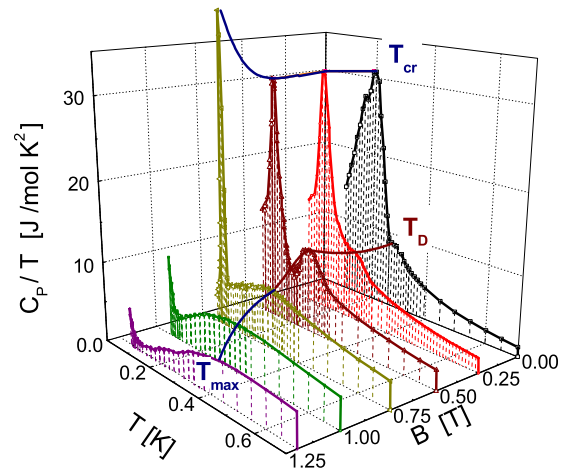

FIG. 6. Specific heat over temperature of YbPd$_2$In at different applied magnetic fields up to 1.2 T in a 3D representation. The upper continuous curve indicates the maximum value of $C_P/T(B)$ defining the critical temperature $T_{\text{cr}}(B)$. Lower continuous curve: at $0 < B <$ 0.75 T it indicates the maximum of the small dome at $T_D \sim 270$ mK. For $B > 0.75$ it traces the field dependent maximum. Vertical lines at 0.7 K are a guide to the eyes for respective field intensities.

be properly fitted with a modified power law: $C_{\text{fit}}(T)/T = 0.5/(T^{2.36} + 0.02)$; see Fig. 5. This power-law dependence strongly resembles that of the compounds YbPt$_2$X ($X =$ In and Sn) [10]. In the case of these Pt homologues C_m/T increases with a similar trend down to ≈ 0.20 K where it practically flattens in YbPt$_2$In and slightly turns down in the case of YbPt$_2$Sn.

The small jump of $\Delta C_m = 53$ mJ/mol K observed at $T = 2.2$ K coincides with the transition temperature of Yb oxide. However, a transition at a similar temperature was reported in YbPd$_2$Sn [17], where it was attributed to a superconductive transition. In order to elucidate whether in the case of YbPd$_2$In this is an extrinsic or intrinsic effect of the sample, we have proceeded to measure the AC susceptibility which is reported in the inset of Fig. 5. From the figure, we see no sign of superconductivity down to 2 K in the case of YbPd$_2$In, therefore we can argue that this transition is likely extrinsic and probably due to Yb oxide.

IV. DISCUSSION

Figure 6 shows the thermal dependence of C_P/T at $0.065 < T < 0.7$ K in fields up to $B = 1.2$ T. The critical temperature $T_{\text{cr}}(B)$ of the magnetic transition decreases linearly with the applied field and extrapolates to $T_{\text{cr}} = 0$ for $B \approx 1$ T. Coincidentally, the upturn at low temperatures for $B \approx 1.2$ T can be described by $1/T^2$ and it can be properly accounted for as being due to nuclear contribution. However, the low-temperature upturn of the measurement at $B \approx 1$ T still contains the tail of the magnetic transition occurring below the measurement limit.

The C_m/T_{cr} anomaly narrows keeping its maximum value of 30 J/mol K^2 up to $B = 0.5$ T but showing a strong increase up to 36.7 J/mol K^2 for $B = 0.75$ T. Further field increase

shifts T_{cr} below the lower experimental limit of temperature but still showing its tail for $B = 1$ T above 65 mK.

From the monotonous decrease of $T_{\text{cr}}(B)$ one may presume that the transition is of antiferromagnetic nature, however its apparent second-order character at $B = 0$ T clearly transforms into a first order at $B = 0.75$ T. Coincidentally, a constant C_m/T_{cr} value is observed up to $B = 0.5$ T; see Fig. 6. This is a typical behavior observed in a number of heavy fermion compounds [18] where the magnetic degrees of freedom involved into the ordered phase (S_{ord}) decrease with the ordering temperature. However, the deviation from such C_m/T_{cr} constancy associates its behavior at $T \to 0$ to the well-known compound exhibiting hidden order URu$_2$Si$_2$ [19]. It worth noting that, in spite of the large difference between their respective critical temperatures and critical fields, there is a striking coincidence in the so-called effective quasiparticle g factor [20], i.e., the ratio between their characteristic parameters $B_{\text{cr}}/T_{\text{cr}}(B = 0) \approx 2$ T/K for URu$_2$Si$_2$ and ≈ 3 T/K for YbPd$_2$In.

The unexpected dome arising at $T_D \approx 270$ mK, just above the transition at $B = 0$ T, increases its intensity up to $B = 0.5$ T without changing the temperature of its maximum. This satellite anomaly vanishes at $B = 1$ T. Coincidentally, a C_m/T maximum at $T_{\text{max}}(B)$ develops and becomes field dependent. Its further increase for $B > 1.5$ T was already analyzed in Fig. 4 in a $C_P(T)$ representation. Although the origin of the domelike anomaly is unknown, its field dependence resembles the one observed in Ce(Co$_{1-x}$Fe$_x$)Si alloys [21] where it was attributed to magnetoelastic effects as precursors of an antiferromagnetic transition.

In order to better describe the field variation of the domelike anomaly at $T_D \approx 270$ mK low-temperature specific-heat results are presented in Fig. 7 in a $C_P(T, B)$ representation up to $T = 1$ K and $B = 1.2$ T. There, one may clearly appreciate that this T_D dome shows a maximum intensity at $B = 0.5$ T and practically vanishes at $B = 0.75$ T. Simultaneously, at
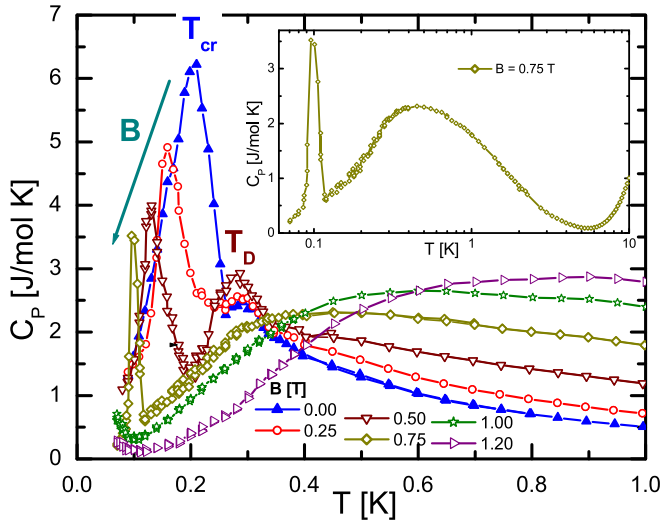
FIG. 7. Temperature dependence of YbPd$_2$In specific heat at different applied magnetic fields up to 1.2 T, showing the $T_{cr}(B)$ decrease and the intensity variation of the dome at $T_D \approx 270$ mK. Inset: $C_P(T)$ dependence in $B = 0.75$ T field in a wider range of temperature to show the relevance of the different anomalies in a semilogarithmic representation.
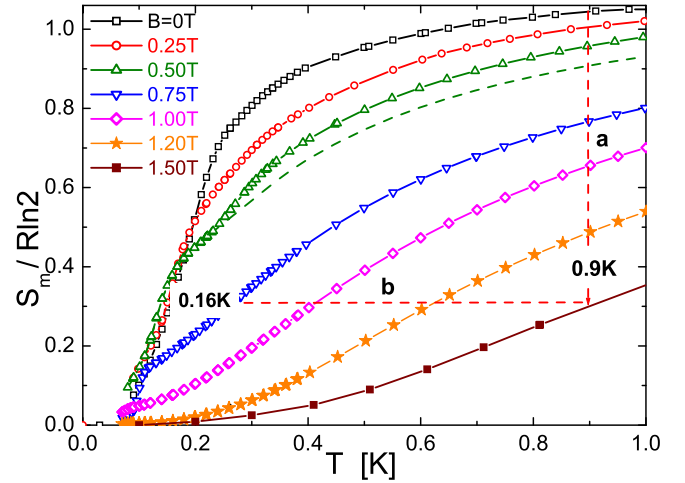

FIG. 8. Thermal variation of the entropy at different applied fields, normalized by the total entropy expected for a doublet ground state: $R \ln 2$. Dashed curve represents the entropy for $B = 0.5$ T after subtracting the 270-mK anomaly contribution. Red dashed lines with arrows indicate a refrigeration path where YbPd$_2$In is first isothermally (0.9 K) magnetized at 1.5 T (a) and then adiabatically demagnetized (b) reaching the final temperature of 0.16 K.

that magnetic field the maximum at $T_{\max}$ starts to develop. In the inset of Fig. 7 the $C_P(T)$ dependence in the $B = 0.75$ T field is presented in a wider range of temperature allowing us to compare the intensity of different anomalies.

As mentioned before, these $C_m(T)$ anomalies can be properly described as Schottky-type anomalies (S_{sch}) only above $B = 4$ T, because they do not reach the expected maximum of $C_{sch} = 3.6$ J/mol K. In spite of this, the maxima can be properly fitted by two $C_{sch}(T)$ type functions of similar weight and slightly shifted in energy among them. This feature reveals that the interaction driving the lower temperature transition is not fully quenched by the magnetic field up to at least $B = 4.5$ T where a single $C_{sch}(T)$ function actually describes the anomalies.

According to Fig. 6, as the transition temperature at $T_{cr}(B = 0) \approx 250$ mK decreases with magnetic field, the magnetic degrees of freedom are progressively transferred to higher temperature with the consequent shift of the maximum slope: $\delta S_m / \delta T = C_m / T$; see Fig. 8. As shown in Fig. 4, the maximum of $C_m / T(B)$ occurs at 1.2 K for $B = 1.5$ T and increases proportional to the field intensity. This relation between the temperature of the maximum ($T_{\max}$) and the intensity of the magnetic field is one of the empirical criteria applicable to the comparison of different Yb-based compounds which behave as very heavy fermions becoming proper candidates to adiabatic demagnetization refrigeration (ADR) [22].

A. Entropy

The low-temperature magnetic contribution to the entropy S_m was obtained integrating $C_m(T)/T$ in temperature. In Fig. 8, the thermal dependence is presented for different magnetic fields up to 1.5 T. In this compound, the extrapolation of C_m/T to $T = 0$ from the lowest measured temperature

(cf. 65 mK) becomes relevant due to the significant entropy increase at very low temperature. The approach chosen to correct this uncertainty was to use a linear extrapolation of $C_m(T)/T$ down to zero at $T = 0$ according to the Nernst postulate ($S_m \rightarrow 0$ for $T \rightarrow 0$). Following this criterion, the entropy reached at 1 K for the zero field measurement slightly overcomes the expected $S = R \ln 2$ value. This excess of entropy can be attributed to the entropy contained in the anomaly at $T_D \approx 270$ mK or to the not considered nuclear contribution. In the former case it would support the proposed magnetoelastic origin of the anomaly. In order to visualize this contribution at its maximum intensity, we have included in Fig. 8 the entropy variation at $B = 0.5$ T after subtracting the T_D anomaly (see dashed curve). For the latter possibility, an unusual nuclear-ground-state coupling mechanism should be accounted for, which is not easy to distinguish in this case.

In Fig. 8 a typical adiabatic demagnetization path is also shown, where the large low-temperature electronic entropy at zero field is partially shifted to higher temperatures by the magnetic field. This large $S_m(B)$ variation allows efficient ADR effect by applying B up to 1.5 T at 0.9 K, and then cooling down to 0.16 K by removing the magnetic field. The efficiency of this process in thermal comparison with other rare-earth intermetallic compounds is analyzed elsewhere [22].

B. Weak magnetic exchange in the framework of magnetic frustration

The question arises about the lack of magnetic order down to about 200 mK whereas many other Yb compounds, showing magnetic moments of similar intensity and interatomic spacing, order more than one decade of temperature above. Recent studies have revealed a significant number of Yb-based intermetallic compounds exhibiting a power-law

dependence above 300 mK [10–13], some of them showing a discontinuity in $C_m(T)/T$ at that temperature, while others show a change of temperature dependence [23]. Two main reasons, which may act simultaneously, can be argued to explain this scenario: magnetic frustration and extremely weak magnetic interactions. In the case of YbPd$_2$In both conditions may converge to inhibit magnetic order down to very low temperature. On the one hand, the edge-sharing tetrahedral coordination of Yb atoms [presented in Fig. 1(b)] provides the geometry for magnetic frustration, like in the spin ice prototype Dy$_2$Ti$_2$O$_7$ [24]. On the other hand, a very weak Yb-Yb magnetic interaction reduces the possibility for long-range magnetic order development. The later scenario is based on the physical properties observed in the YbPt$_2$X homologues [10]. It is known that in intermetallic compounds the dominant mechanism governing the magnetic exchange is the conduction electrons-mediated Ruderman-Kittel-Kasuya-Yosida (RKKY) interaction, which depends on the coupling parameter J_{ex}, the density of states of the oscillatory spin polarized band $\delta(E_F)$, and inversely to the interatomic distance $f(1/d^3)$. The strength of J_{ex} can be evaluated from the low-temperature value of $|\theta_P|_{T\to 0} \approx -2$ K, extracted by fitting $1/\chi$ ($T < 10$ K).

This number, together with the lack of any Kondo interaction symptom, also point to very weak J_{ex} intensity. An empirical evaluation of the weight of the $\delta(E_F)$ factor can be extracted from the Sommerfeld coefficient: $\gamma \sim$ 6 mJ/mol K^2, of LuPd$_2$In reported in Ref. [25]. This is a small value considering that the formula unit contains four atoms, whose respective individual γ values add up to more than 30 mJ/mol K^2. The Yb-Yb spacing, $(d_{\text{Yb-Yb}}) = 4.7$ Å, may also become a significant factor for the weak effective interaction. Therefore the weakness of each one of these RKKY parameters and their multiplicative character point to an extremely weak RKKY interaction.

C. Phase diagram

A magnetic phase diagram is presented in Fig. 9 which contains the field dependence of the phase boundary T_{cr} and the temperature of the dome T_D. The entropy collected at $0 \leqslant T \leqslant T_{cr}(B)$, that accounts for the degrees of freedom condensed into the ordered phase S_{MO}, is also included. The circle at $T_{cr}(B = 1$ T) represents an extrapolation of the $T_{cr}(B < 1$ T) curve. Although it placed below the lower accessible temperature ($T = 65$ mK), a turn up of the $C_m/T (B = 1$ T) curve (see Fig. 6) reveals the reminiscence of that transition below that temperature.

In Fig. 6, $T_D(B < 0.75$ T) and $T_{max}(B > 0.75$ T) trajectories seem to coincide in a single curve. However, the detailed magnetic phase diagram shows that the constant $T_D = 270$ mK and the field dependent T_{max} simply converge to a point at around $B_D \approx 0.8$ T. There the degrees of freedom related to the "dome" contribution vanish in coincidence with the arising $T_{max}(B)$ anomaly [see the $T_{max}(B)$ trajectory up to $B = 1.5$ T on the right axis of Fig. 9]. Although this feature indicates that these two contributions are of a different nature, such coincidence reveals a change in the ground-state (GS) properties at B_D.
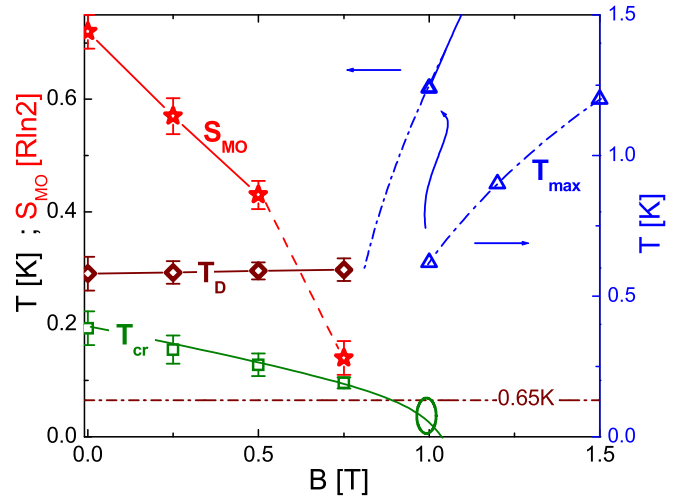

FIG. 9. Magnetic phase diagram as a function of applied field showing: on the left axis, the ordering temperature T_{cr}, the entropy gain within the ordered phase S_{MO} and the temperature of the dome T_D. Continuous (green) curve is a guide to the eyes for the $T_{cr}(B) = 0$ and the ellipse represents an extrapolated point at $B = 1$ T. The dash-dot line at 65 mK indicates the thermal experimental limit. Continuous line (red) in $S_{MO}(B)$ covers the second-order-type transitions while the dashed segment extrapolates to the first-order one. On the right axis, the temperature of the maximum of $C_m/T (T_{max})$ is presented. The extrapolation of $T_{max}(B)$ to $B < 1$ T (dashed-dot blue line) is compared with the $T_D(B)$ using the left axis scale as indicated by the left-pointing blue arrow.

An important question concerns the change of the nature of the T_{cr} transition from second-order type to first order at 0.5 T $< B <$ 0.75 T, as shown in Fig. 6. As mentioned before, this occurs after showing a constant $C_m/T_{cr} \approx 30$ J/mol K^2 value up to $B = 0.5$ T, which suddenly increases up to ≈ 36.7 J/mol K^2 at $B = 0.75$ T. This type of behavior has been typified in a systematic analysis of low-temperature magnetic phase diagrams of Ce compounds, performed to distinguish between different $S_{MO}(T \to 0)$ trajectories observed in magnetically ordered phases [26]. From the $C_m/T(B)$ behavior of YbPd$_2$In observed in Fig. 6, this compound can be included into the group whose $S_{MO}(T_{cr})$ values exceed those allowed by the law of corresponding states, cf. those whose $S_{MO} \to 0$ along with $T_{cr} \to 0$. Therefore, the systems with $S_{MO}|_{\to 0} > 0$ are constrained by the third law of thermodynamic to undergo a first-order transition in a critical point in order to reduce the $S_{MO}(B)$ value. In the present magnetic phase diagram one may appreciate that, although both $T_{cr}(B)$ and $S_{MO}(B)$ extrapolate to zero, the latter drops faster than expected at $B = 0.75$ T in coincidence with the first-order character of that transition.

The exemplary cases for this situation are as a function of field URu$_2$Si$_2$ [19] and PrFe$_4$P$_{12}$ [27], and as a function of chemical potential, the Ni rich Ce$_2$(Ni$_{1-x}$Pd$_x$)$_2$Sn [28]. In all these cases, respective second-order magnetic transitions transform into a first-order one where the entropy is suddenly reduced, otherwise $S_{MO} \neq 0$ at $T = 0$. Both URu$_2$Si$_2$ and Ce$_2$(Ni$_{1-x}$Pd$_x$)$_2$Sn show the formation of exotic phases around $T \to 0$ which cannot be excluded for YbPd$_2$In.

V. CONCLUSIONS

The synthesized cubic Heusler YbPd$_2$In compound was characterized in its structural, magnetic, thermodynamic, and transport properties. At high temperatures the Yb atoms were found in their trivalent Yb^{3+} state. The absence of a significant Kondo effect is demonstrated by the very low value of θ_P and by the continuous decrease of the electrical resistivity with temperature.

At low temperatures this compound shows its relevant properties with a very high $C_m/T \approx 30$ J/mol K^2 value at $T \approx 250$ mK, reached after a power-law increase of $C_m(T)/$T which collects nearly 1/2 of the doublet GS entropy. The formation of a long-range magnetic order parameter down to a very low temperature is prevented in this compound by two characteristics which may act simultaneously: the structural conditions for magnetic frustration and a very weak exchange interaction. Under magnetic field, the $C_m(T, B)$ behavior is properly described by a simple two-level scheme only for $B > 4$ T where the applied field is strong enough to quench the low-energy magnetic correlations. At that point the GS degeneration is fully removed by Zeeman splitting.

Since this compound and other homologues show a transition around $T^* = 250$ mK, it is evident that the weak interaction responsible for the transition is progressively overcome by the applied field. The removal of the GS degeneracy by magnetic field produces a significant shift of the entropy to higher temperatures. This simple scenario may explain why YbT_2X compounds ($T =$ Pd, Pt and $X =$ In, Sn) are promising materials for adiabatic demagnetization in cooling processes.

[1] F. Steglich and S. Wirth, Rep. Prog. Phys. **79**, 084502 (2016).

[2] P. Carretta, M. Giovannini, M. Horvatic, N. Papinutto, and A. Rigamonti, Phys. Rev. B **68**, 220404(R) (2003).

[3] L. S. Wu, W. J. Gannon, I. A. Zaliznyak, A. M. Tsvelik, M. Brockmann, J.-S. Caux, M. S. Kim, Y. Qiu, J. R. D. Copley, G. Ehlers, A. Podlesnyak, and M. C. Aronson, Science **352**, 1206 (2016).

[4] P. Carretta, R. Pasero, M. Giovannini, and C. Baines, Phys. Rev. B **79**, 020401(R) (2009).

[5] M. Giovannini, R. Pasero, and A. Saccone, Intermetallics **18**, 429 (2010).

[6] F. Gastaldo, M. Giovannini, A. Strydom, R. Djoumessi, I. Čurlík, M. Reiffers, P. Solokha, and A. Saccone, J. Alloys Compd. **694**, 185 (2017).

[7] T. Muramatsu, T. Kanemasa, T. Kagayama, K. Shimizu, Y. Aoki, H. Sato, M. Giovannini, P. Bonville, V. Zlatic, I. Aviani, R. Khasanov, C. Rusu, A. Amato, K. Mydeen, M. Nicklas, H. Michor, and E. Bauer, Phys. Rev. B **83**, 180404(R) (2011).

[8] H. Yamaoka, N. Tsujii, M.-T. Suzuki, Y. Yamamoto, I. Jarrige, H. Sato, J.-F. Lin, T. Mito, J. Mizuki, H. Sakurai, O. Sakai, N. Hiraoka, H. Ishii, K.-D. Tsuei, M. Giovannini, and E. Bauer, Sci. Rep. **7**, 5846 (2017).

[9] E. Bauer, G. Hilscher, H. Michor, C. Paul, Y. Aoki, H. Sato, D. Adroja, J.-G. Park, P. Bonville, C. Godart, J. Sereni, M. Giovannini, and A. Saccone, J. Phys.: Condens. Matter **17**, S999 (2005).

[10] T. Gruner, D. Jang, A. Steppke, M. Brando, F. Ritter, C. Krellner, and C. Geibel, J. Phys.: Condens. Matter **26**, 485002 (2014).

[11] I. Čurlík, M. Giovannini, J. G. Sereni, M. Zapotokova, S. Gabáni, and M. Reiffers, Phys. Rev. B **90**, 224409 (2014).

[12] M. Giovannini, I. Čurlík, F. Gastaldo, M. Reiffers, and J. G. Sereni, J. Alloys Compd. **627**, 20 (2015).

[13] J. G. Sereni, Physica B **536**, 357 (2018).

[14] Y. Tokiwa, B. Piening, H. S. Jeevan, S. L. Bud'ko, P. C. Canfield, and P. Gegenwart, Sci. Adv. **2**, e1600835 (2016).

[15] M. Babateen, J. Crangle, F. Fauth, K.-U. Neumann, and K. R. A. Ziebeck, Physica B **213–214**, 300 (1995).

[16] W. Kraus and G. Nolze, J. Appl. Crystallogr. **29**, 301 (1996).

[17] Y. Aoki, H. R. Sato, H. Sugawara, and H. Sato, Physica C **333**, 187 (2000).

[18] J. G. Sereni, J. Low Temp. Phys. **179**, 126 (2015).

[19] M. Jaime, K. H. Kim, G. Jorge, S. McCall, and J. A. Mydosh, Phys. Rev. Lett. **89**, 287201 (2002).

[20] N. Harrison and M. Jaime, arXiv:1902.06588.

[21] V. Correa, D. Betancourth, J. Sereni, N. Caroca Canales, and C. Geibel, J. Phys.: Condens. Matter **28**, 346003 (2016).

[22] J. G. Sereni, arXiv:1807.08742, [Philos. Mag. (to be published)].

[23] J. G. Sereni, J. Low Temp. Phys. **190**, 1 (2018).

[24] A. P. Ramirez, A. Hayashi, R. J. Cava, R. Siddharthan, and B. S. Shastry, Nature (London) **399**, 333 (1999).

[25] D. Jang, T. Gruner, A. Steppke, K. Mitsumoto, C. Geibel, and M. Brando, Nat. Commun. **6**, 8680 (2015).

[26] J. G. Sereni, Philos. Mag. **93**, 409 (2013).

[27] T. D. Matsuda, H. Okada, H. Sugawara, Y. Aoki, H. Sato, A. V. Andreev, Y. Shiokawa, V. Sechovsky, T. Honma, E. Yamamoto, and Y. Onuki, Physica B **281–282**, 220 (2000).

[28] J. G. Sereni, G. Schmerber, M. G. Berisso, B. Chevalier, and J. P. Kappler, Phys. Rev. B **85**, 134404 (2012).